Mechanical behaviour of fully densified silica glass under Vickers indentation

V. Keryvin, L. Charleux, R. Hin, Jean-Christophe Sangleboeuf, J.-P. Guin

Accepted Manuscript

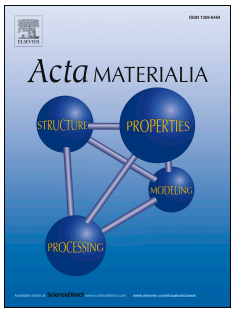

Mechanical behaviour of fully densified silica glass under Vickers indentation

V. Keryvin, L. Charleux, R. Hin, J.-P. Guin, J.-C. Sangleboœuf

PII: S1359-6454(17)30187-8

DOI: 10.1016/j.actamat.2017.03.008

Reference: AM 13614

To appear in: *Acta Materialia*

Received Date: 9 November 2016

Revised Date: 10 February 2017

Accepted Date: 5 March 2017

Please cite this article as: V. Keryvin, L. Charleux, R. Hin, J.-P. Guin, J.-C. Sangleboœuf, Mechanical behaviour of fully densified silica glass under Vickers indentation, *Acta Materialia* (2017), doi: 10.1016/j.actamat.2017.03.008.

Mechanical behaviour of fully densified silica glass under Vickers indentation

V. Keryvin[a,c,*], L. Charleux[b], R. Hin[a,c], J.-P. Guin[c], J.-C. Sangleboœuf[c]

[a]*Univ. Bretagne-Sud, FRE CNRS 3744, IRDL, F-56321 Lorient, France*
[b]*Univ. Savoie Mont Blanc, EA 4114, SYMME, F-74000 Annecy, France*
[c]*Univ. Rennes 1, UMR CNRS 6251, IPR, F-35042 Rennes, France*

Abstract

When subjected to constrained deformation loadings, such as during an indentation test, silica glass experiences complex deformation mechanisms including densification and volume-conservative shear plasticity. The densification mechanism may increase the density up to more than 21%. The question of the mechanical behaviour of an already fully densified glass sample naturally arises. This issue is one of the key points to address when one tries to propose a constitutive model of pristine silica glass. Indeed, during an indentation test, which is a popular test for this task, beneath the indenter tip, some regions might be fully densified. What is their behaviour, after saturation in densification and during loading, is therefore an issue to address. Moreover, this is a crucial point for exploring the transition from plasticity to cracking, which is of paramount importance and a long-term objective for predicting the lifetime of glass products subjected to contact loadings such as impact or scratching.

In this paper, a quantitative identification of fully densified silica mechanical constitutive behaviour is made by using instrumented indentation testing and finite element analyses. The use of such an indirect method to assess the

mechanical behaviour of this material comes from its brittleness behaviour in unconstrained deformation modes usually employed in metals plasticity. It is shown here that fully densified silica behaves as a von Mises material (rate-independent shear plasticity without strain-hardening) like some crystalline metals. The yield strength and yield strains are, at the contrary, much higher than for alloys: respectively 6.5 GPa and 6.1 %. This mechanical modelling, as well as the plastic parameters values found, are in excellent agreement with very recent experimental and numerical simulations on silica glass and silicate glasses.

The high value of the yield strain is found to explain unusual indentation features such as a unusual long range residual piling-up while sinking-in is predicted during loading, as well as low values of the ratio hardness-to-yield strength.

Keywords: Non-metallic glasses (silicates); Plasticity; Constitutive modelling; Densification; Nanoindentation.

1. Introduction

Silica glass (SiO_2) ~~may be viewed as the archetype of a three dimensional network glass former. It~~ is a highly brittle material that breaks in bending under few tens of MPa because of its extreme sensitivity to surface damage [1, 2]. Yet, under constrained mechanical loadings such as hydrostatic tests or indentation, it can deform permanently without breaking or even cracking [3, 4]. Under pure hydrostatic conditions, its density (respectively its volume) may increase permanently [5, 6, 7] by more than 20 % (respectively

*Corresponding author: vincent.keryvin@univ-ubs.fr

decrease by more than 16 %) [3, 8]. This has been related to some changes in the intermediate range order, among which the decrease of intertetrahedra angles [9], and is referred to as pressure-induced densification (PID). It is now recognised that during indentation, densification occurs as well as volume conservative shear flow [10]. These main mechanisms at stake have been observed separately and very recently properly modelled: PID as recalled previously [11] and shear flow by uniaxial compression experiments [12, 13]. For the former mechanism (PID), the authors proposed a description of the densification process with a threshold pressure for the onset of densification, an increase of densification upon pressure, and another pressure threshold for the saturation in densification. They also pointed out the necessity to use a Finite Deformation framework and to account for the elastic stiffening with densification (for instance the bulk modulus will double) [11]. As for the latter mechanism, the authors of Ref. [12, 13], using compression tests on micropilars, showed that silica glass behaves in compression as a perfectly elasto-plastic material (without any strain hardening in shear) with a compressive yield strength around 6-7 GPa. These two mechanisms take place together during an indentation test [14, 15] so that their kinetics must be related to a combination of driving forces (shear and pressure). Different authors have proposed such constitutive modellings that are successful in describing the mechanical response of the instrumented indentation test (the force-displacement curve) [16, 17, 18, 19, 20]. Some of them were also successful in observing densification fields beneath the residual imprint by Raman spectroscopy [21, 18] or by a chemical dissolution technique [22].

However, a piece of this jigsaw puzzle is still missing: what does the behaviour of the material become when the densification is saturated to $\sim 21\%$

? In other words, what is the mechanical behaviour of fully densified silica glass? This issue is of paramount importance not only from a condensed-matter physics point of view but also since the ultimate target of modelling the mechanical response of glasses to surface damage is to describe the transition from plasticity to cracking and it is highly liable that these densified or fully densified zones play a major role in it.

This is the current objective of this paper. We will analyse instrumented indentation tests, in terms of force-displacement curves and residual imprints, to propose an adequate description of the mechanical behaviour of fully densified silica glass under Vickers indentation.. The paper is organised as follows. We will first describe how silica glass samples are densified up to more than 21%, how indentation tests are performed and how results are analysed. The numerical procedures, using both two- and three-dimensional finite element analyses of the Vickers indentation test, will be then described. After presenting and analysing both experimental and numerical results, we will eventually challenge our findings in terms of mechanical modelling and material properties to very recent experimental and simulation literature results.

2. Experimental and numerical methods

2.1. Material and experimental procedures

Silica glass (Vitreosil^{TM}, Saint-Gobain, France) specimens (0.6 mm in diameter and 2 mm in length) were densified by means of an octahedral multi-anvil apparatus using a Walker cell. A typical run consisted in raising the load pressure of the main ram at a rate of 0.5 MPa/min of oil up to obtaining a pressure of 25 GPa on the sample. After reaching the target pressure, the specimens were maintained at high pressure for one hour and then slowly

unloaded. Density was measured with a better than 0.001 g/cm^3 accuracy by means of a density gradient method using two partially miscible liquids (iodobenzene and methylene iodide). The density of the pristine samples was 2.2 g/cm^3. After unloading from the Walker cell, samples had a density increased by 21.6 %. They are further referred to as fully densified (FD). Further details may be found elsewhere [3].

Instrumented indentation tests (IIT) were carried out with a micro-indenter testing device (Fischerscope H100 XYp, Fischer, Germany) at ambient conditions (23˚C and 55% relative humidity). It has a load resolution of 0.02 mN and a depth resolution of 2 nm. The calibration of the instrument was done by using ISO-14577 standard on a reference block (BK7^{TM} borosilicate glass). The indenter tip is a Vickers diamond pyramid. IIT tests were carried out both on a pristine silica sample (further referred to as PS, studied for sake of comparison) and on FD. A typical '4-5-4' loading sequence was used: 4 s to reach the maximum force P_m, 5 s of holding time, and 4 s to unload the sample's surface. They were force-controlled and the P_m values were 100 mN. The mechanical response of the indentation test is the force P vs. the displacement δ (counted positively). Due to the high reproducibility of the indentation test on the glass surface, five indents per chosen maximum load were performed. Unloading curves were analysed to extract an indentation modulus, M, and an indentation hardness, H_{IT}, by Oliver and Pharr's method [23].

Atomic force microscopy made it possible to record the three-dimensional geometry of the residual indentation imprint after unloading. Images were captured by using the contact mode of an AFM (Bruker Nanoscope V, Dimension 3100, Santa Barbara, CA) equipped with silicon nitride tips (DNP) with a nominal tip radius of the order of 20 nm and apical angle of 40°. The AFM

tip being much sharper than the Vickers indenter it ensures that the residual imprint shape is captured without AFM probe shape convolution effect. Finally, the piezo scanner was calibrated in X-Y-Z directions with a grid having a 10 μm pitch (X-Y directions) of 200 nm deep squared holes (Z direction).

Regarding image post treatment, the size of the scanned areas containing an indentation imprint was large enough so that a sufficient area, unaffected by the indentation process, surrounds the imprint and may be used as a reference surface for post treatment. This surface of reference was extracted from the raw image by using a disk-shaped mask centered on the imprint. It was assumed that the surface of the tested samples, far from the indentation imprint, was flat (i.e. no tilt and no offset). Thus a linear fit was applied to this data set, which was subsequently subtracted from the raw image. It is important to note that removing a tilt on the whole data set does not modify the three-dimensional shape of the residual imprint. Meyer's hardness, H, was also measured as the ratio P_m to the projected contact area, after unloading, on the residual imprints.

2.2. Numerical procedures

Finite element analyses (FEA) of the indentation process were performed using both two (2D) and three dimensional (3D) models constituted of a sample and an indenter. The 3D mesh is generated from a coarser 2D mesh. The 2D mesh is first described.

The sample's mesh is divided into a core zone, beneath the indenter tip, where the mesh is fine, and a shell zone where the mesh is coarse far from the contact. The core zone is itself divided into a square zone with a 32x32 (2D) or 16x16 (3D) quadrangular structured mesh contained into an outer un-

structured zone made of quadrangular elements (32/16 again along the axis $z = 0$). The shell zone is decomposed into a transition zone where the element size is progressively increased and a outer zone, both with quadrangular elements. All elements are linear and use full integration [1]. The dimensions of the mesh are chosen in order to minimise the effect of the far-field boundary conditions. This is made by using a sufficient number of outer elements in the shell zone. The typical ratio of the maximum contact radius and the sample size is about 2×10^3. The 3D model relies on 45° swept 2D meshes since the Vickers pyramid has symmetries so that only $1/8^{\text{th}}$ of it has to be meshed. The resulting elements are eight-node hexahedrons except along the axis where linear six-node prismatic elements are used. Detailed views of the meshes are shown in Figure 1.

As for the indenter, the same procedure used for the sample mesh is employed. For 2D simulations, a triangle with an half-angle of 70.23° (equivalent angle of the Vickers pyramid) is meshed. For 3D models, a triangle with an half-angle of 68° is first meshed before being swept.

The indenter material (diamond) is assumed to be isotropic, linear elastic (Poisson's ratio ν_i of 0.07 and Young's modulus E_i of 1140 GPa [23]). The contact between the indenter and the sample's surface is strict (Signorini conditions) and taken as frictionless. The contact zone and potential piling-up will take place along the square elements of the core zone. The boundary conditions consist of a null radial displacement along the vertical axis for both the sample and the indenter and a null displacement on the outer nodes of the sample. The force on the indenter, P (taken as positive), is controlled and the displacement of the indenter far from its tip, δ (counted positively), is

[1] No evidence of possible volumetric locking beneath the indenter tip has been observed.

recorded. The experimental maximum force was $P_m = 10$ mN[2] . The problem is solved using the commercial software ABAQUS^{TM} (version 6.15). The pre- and post-processing tasks were made with Abapy toolbox [24]. ~~Details and views of the meshes are also visible in the documentation associated with Ref. [24].~~

The mechanical behaviour of the densified silica glass is assumed to be elasto-plastic (rate-independent) with a linear isotropic elasticity (Young's modulus E and Poisson's ratio ν). The plastic part, topic of this investigation, will be addressed hereinafter The finite strains framework is employed.

3. Results

3.1. Experimental results

The curves $P - \delta$ of both PS and FD specimens are shown in Figure 2. FD is obviously much stiffer than PS. At a given load, the penetration depth is lower during the loading stage. Because of geometrical similarity of sharp indentation [25, 26], the loading part of the curves is a parabola whose curvature C is the indentation loading stiffness[3]. Values for both specimens are reported in Table 1, and it can be seen that FD is 44 % stiffer than PS. After unloading, the residual penetration depth, δ_f, is consistently lower for FD *vis-à-vis* PS. The ratio of the reversible work released during unloading, W_r, to the total work involved during loading, W_t, is also indicative of the

[2]Actually only $P_m/8$ is imposed because of the symmetries reported hereinbefore, for the 3D mesh.

[3]Actually, it is not a stiffness, and this why it is called the loading pre-factor usually. Indeed the stiffness is the slope of the $P - \delta$ curve, which is then $C \times \delta$, so a linear stiffness. Still, taking aside the kinematics δ, the parameter of interest describing the stiffness is C.

indentation response. This ratio is 18% higher for FD than for PS. This might qualify it as "more elastic" than pristine silica.

The indentation modulus, M, is also reported in Table 2. The contribution of the indenter stiffness was subtracted and, for linear isotropic cases, M is $E/(1-\nu^2)$. Elastic parameters of densified samples have been characterised in literature [27, 28]. Taking the average reported value of 0.22 for ν and the M value from this work, E is found to be 106 GPa,which is in the range 110 ± 6 GPa reported in literature [28]. These elastic parameters are reported in Table 2.

The residual imprints are shown in Figure 3 along with the profiles extracted along the four edges and the four faces. All imprints on FD were free of cracks, while edge cracks (quasi circles around the imprint, on the faces, see Ref. [29**?**] for a detailed description of cracking systems in silica glass) were observed for PS. PS exhibits a sinking-in phenomenon, since all residual depths are below the reference level of the initial surface of the sample. The profiles extracted (where the contribution of a edge crack is noticeable) confirm this. As for FD, the opposite situation is observed. An unusual long range piling-up is visible where the matter is above the initial reference level at a distance up to $\sim$ 3 µm from the imprint center. This is the case along the faces but also along the edges, which is rather singular for an inorganic glass. Usually, we can have piling-up along the faces on some silicate glasses [4] but not along the edges. For metallic glasses, piling-up may be even more pronounced but only along the faces [30, 31], not along the edges. This is therefore quite a rather unique situation for this fully densified silica glass.

3.2. Numerical results

Since the fully densified silica glass may not densify anymore, it sounds logical to assume first that the only mechanism for permanent deformation is volume-conservative plastic flow. The subsequent absence of any strain hardening mechanism in shear [13, 32] made us use a von Mises material for describing the behaviour of FD, *i.e.* a rate-independent elasto-plastic model without strain hardening with the second invariant of the deviatoric part of the stress tensor (the von Mises equivalent stress) acting as the sole driving force. No contribution of the two other invariants is considered. In this simple model, the only plastic parameter is the yield strength σ_y. We then performed a straightforward identification procedure by minimising the gap between the simulated force-displacement curve and the experimental one (from Figure 2) with this plastic parameter as the only free variable[4]. A remarkable agreement is found for $\sigma_y = 6.5$ GPa, as observed in Figure 4.

Material parameters are presented in Table 2. Due to elastic stiffening, the compressive yield strain is strongly decreased, by 40 %, when comparing FD to PS.

4. Discussion

Molecular dynamic simulations (MD) have proven to be relevant tools for examining the multiaxial response of silica glass to mechanical testing, which is usually uneasy experimentally. Analysing the results in terms of driving forces (shear, pressure) versus mechanisms (densification, shear flow,...)

[4] We must mention that this procedure suffers from non uniqueness when two or more parameters are to be identified. This is not our case where only one parameter is determined, as pointed out in [26, Fig. 7].

might give some insight on the choice of a given constitutive modelling a the continuum level, as well as the modifications in the short-to-medium range order. Yuan and Huang [33] found that shear flow in densified silica can be attributed to a less rigid local environment associated with 5-fold Si coordination defects, more amenable to local shear deformation as compared with the 4-fold coordination state. Very recently, Molnar *et al.* [32] conducted MD simulations on binary NaO-SiO_2 glasses and observed that the shear yield strength was unaffected by the densification process. In both cases, the mechanical behaviour of fully densified glasses was found to be adequately described by pressure-dependent yield criteria such as Drucker-Prager (when pressure is an additional driving force) or extended Drucker-Prager (with the third stress invariant acting as another additional driving force). This situation ressembles that of some metallic glasses or polymeric glasses whose behaviour has been described by such models [34, 35, 36, 37]. These models involve a higher number of plastic parameters, in terms of yield criterion and plastic flow rule, than for the von Mises model we have used and for which only σ_y is required. What is remarkable is that this latter simple model suffices to describe quite perfectly the mechanical response of the indentation test on FD. MD simulations (again very recent) in Ref. [38], on pure silica glass, indicated that the shear yield strength was also unaffected during the densification process. Our present work as well as experimental results published in the literature [13] are very consistent with this statement. Indeed, experimental values reported in Table 2 show that the yield strength of PS and FD samples is the same.

Usually, the classical method for analysing the unloading stage of the force-displacement curve [23] fails in extracting the correct indentation mod-

ulus (or Young's modulus provided Poisson's ratio is known) when piling-up occurs. Indeed, piling-up makes this method underestimate the contact area ($\sim$ 30 % for a Zr-base metallic glass [4]) and therefore overestimates the indentation modulus. Yet our indentation results are very consistent with literature ones in terms of elastic parameters. We examine the reasons for this possible discrepancy by FEA. In Figure 5, are compared the numerical profiles along the edges and the faces to the experimental profiles. The comparison is again very satisfactory, excepted at the indentation imprint apex where a discrepancy is visible. The later may result from the finite size of the experimental indenter (tip roundness and truncated length) as AFM probe tip shape effect may be ruled out due to its much sharper geometry. Apart from this very localised zone, the profiles are well described and the residual piling-up along both the faces and the edges are correctly assessed. Thanks to FEA, we have also plotted the profile at maximum load, therefore before unloading. We can observe that a massive sinking-in develops during loading so that the residual piling-up is not a direct consequence of shear flow but rather of the elastic spring-back of the loaded surface during the unloading stage. This means that it is relevant to use the classical method for extracting the indentation modulus and this is why our values are in total agreement with literature results. A more precise comparison between experimental data and numerical simulations is shown in Figure 6. It is a topography view of the residual imprint. Apart from the red part (right), the comparison is very relevant. As for the red part, it shows that the numerical simulation underestimates the pile-up height, maybe due to a small local tilt of the sample since this red part is not present along the four faces of the imprint. We believe that this discrepancy can be ruled out by performing enhanced simulations with a much finer mesh

in the core zone, but this is not the topic of the present work.

To go a step further on this issue, we must now refer to results from a numerical benchmark proposed by Charleux *et al.* [4] with two different classical constitutive equations (Hollomon and Drucker-Prager) to extend this observation. Using the same procedure, we can get some insight on possible piling-up and sinking-in both during loading and loading. This is made (in 2D) for the sole Hollomon model with a strain hardening coefficient $n = 0$ corresponding to the von Mises model, which was shown earlier in this work to be a relevant candidate to quantitatively describe the mechanical response of FD to the indentation test (cf. Figures 4 and 5). Results are presented in Figure 7. It is observed, that up to a yield strain ϵ_y of $\sim$ 1% piling-up occurs both during loading and unloading. After this value, sinking-in prevails during loading while piling-up is always observed after unloading, even if it decreases to very low values as ϵ_y increases. The case for FD corresponds to an experimental value of $\epsilon_y = 6.1\%$; it is superimposed and matches very well the numerical results.

The classical relationship between hardness and compressive yield strength [25] is $H \approx c\,Y$ (Tabor's rule-of-thumb), where Y is the yield strength of the material for a given representative strain. For non strain hardening materials, it is σ_y. For crystalline metals, c, the constraint factor, is taken as 3 and is frequently used as a convenient rule-of-thumb. Actually, this is strictly speaking between Vickers's hardness H_v and σ_y [25]. There is a $\sim$ 7% difference between H and H_v, so $c \sim 2.8$. As reported in Table 2, this ratio is $\sim$ 1.25 for PS and 1.9 for FD. While it can be be treacherous to use Tabor's rule for a material like PS exhibiting an additional densification mechanism under indentation, this should be quite straightforward for FD since it is adequately modelled by

a von Mises material. Yet, for FD, the ratio hardness-to-yield strength is much lower than Tabor's rule. If this number of 2.8 has been revisited since the original work of Tabor, the recognised values nowadays range from 2.6 to 2.7 [39]. It has been shown that for pressure-sensitive glasses, like metallic glasses or polymeric glasses, this ratio can be higher [40, 41, 37]. However, for FD this ratio is much lower than the value for pressure-insensitive materials like metals. Using FEA (2D), we have plotted in Figure 8, the ratio hardness-to-yield strength (H/σ_y) for von Mises materials (for $\nu = 0.22$) as a function of the yield strain ϵ_y in the particular situation where the indenter is of Vickers type. For this indenter, the so-called indentation strain $\epsilon_i = \text{cotan}\,\theta$, where θ is the half angle of the equivalent cone (here 70.27°), is 0.358. Classically we have two regimes described for example in Ref. [26]: a fully plastic regime, for low values of ϵ_y, corresponding to a plateau value of ~ 2.65, the so-called constraint factor c; and an elasto-plastic regime where H/σ_y is lower than c. The experimental case of $\epsilon_y = 6.1\%$ for FD is superimposed on Fig. 8, and matches very well with the numerical results. This indicates, that when using a Vickers indenter, we are still in the elasto-plastic regime of indentation for FD, explaining the low value of the ratio hardness-to-yield strength, which is not in this case the constraint factor defined for the sole fully plastic regime of indentation. The Vickers indenter is not sharp enough to reach this latter regime.

5. Concluding remarks

We have characterised the mechanical properties (elastic stiffness, hardness) of a fully densified silica glass samples (21.6 % increase in density) by using instrumented indentation testing. We have also shown that the ma-

terial's response to Vickers indentation (force-displacement curve, residual imprint) is correctly assessed by a constitutive equation usually relevant for some crystalline metals, *i.e.* a rate-independent pressure insensitive elasto-plastic model without strain-hardening, usually referred to as a von Mises material. This singular comparison with metallic alloys ends rapidly since the yield strength and yield strain values (respectively 6.5 GPa and 6.1 %) are far higher than those for crystalline alloys. These values are in agreement with very recent experimental and simulation studies on densified silica or silicate glasses. Apparent disagreement with indentation features (a perfect assessment by the Oliver and Pharr's method of Young's modulus in the presence of a massive piling-up around the residual imprints ; a ratio hardness-to-yield strength of 1.9 much lower than the constraint factor of ~ 2.7 for crystalline alloys) have been explained again by the very high value of the yield strain. Indeed, finite element analyses have shown that, during the loading stage of indentation, a massive *sinking-in* occurs and it is because of the very high elastic spring-back that unusual (as compared to classical alloys or metallic glasses) piling-up is observed around the residual imprints. The same analyses have highlighted that the material is in the so-called elastoplastic indentation regime and not in the fully plastic one, for this Vickers indenter, where a hardness-to-yield strength value of ~ 2.7 is expected.

This mechanical description of fully densified silica glass mechanical behaviour under Vickers indentation, to our opinion, paves the way for new insights into the constitutive modelling of pristine silica glass during indentation loading, which is a key to understand the transition from plasticity to cracking in these oxide glasses to increase their use in service lifetime.

Acknowledgements

We would like to thank H. Ji (Univ. Rennes 1, France), T. Hammouda (Univ. Blaise Pascal, France) for experimental help and T. Rouxel (Univ. Rennes 1, France) for stimulating discussion.

References

[1] A. A. Griffith, The Phenomena of Rupture and Flow in Solids, Philos. Trans. R. Soc. A Math. Phys. Eng. Sci. 221 (1921) 163–198.

[2] E. Le Bourhis, Glass, Wiley-VCH Verlag GmbH & Co. KGaA, Weinheim, Germany, 2014. doi:10.1002/9783527679461.

[3] T. Rouxel, H. Ji, V. Keryvin, T. Hammouda, S. Yoshida, Poisson's Ratio and the Glass Network Topology - Relevance to High Pressure Densification and Indentation Behavior, Adv. Mater. Res. 39-40 (2008) 137–146.

[4] L. Charleux, V. Keryvin, M. Nivard, J.-P. Guin, J.-C. Sangleboeuf, Y. Yokoyama, A method for measuring the contact area in instrumented indentation testing by tip scanning probe microscopy imaging, Acta Mater. 70 (2014) 249–258.

[5] P. W. Bridgman, I. Simon, Effects of Very High Pressures on Glass, J. Appl. Phys. 24 (1953) 405–413.

[6] H. M. Cohen, R. Roy, Effects of Ultra high Pressures on Glass, J. Am. Ceram. Soc. 44 (1961) 523–524.

[7] J. D. Mackenzie, High-Pressure Effects on Oxide Glasses: II, Subsequent Heat Treatment, J. Am. Ceram. Soc. 46 (1963) 470–476.

[8] T. Deschamps, A. Kassir-Bodon, C. Sonneville, J. Margueritat, C. Martinet, D. de Ligny, A. Mermet, B. Champagnon, Permanent densification of compressed silica glass: a Raman-density calibration curve., J. Phys. Condens. Matter 25 (2013) 025402.

[9] B. Hehlen, Inter-tetrahedra bond angle of permanently densified silicas extracted from their Raman spectra., J. Phys. Condens. Matter 22 (2010) 025401.

[10] T. Rouxel, H. Ji, J. P. Guin, F. Augereau, B. Rufflé, Indentation deformation mechanism in glass: Densification versus shear flow, J. Appl. Phys. 107 (2010) 094903.

[11] V. Keryvin, J.-X. Meng, S. Gicquel, J.-P. Guin, L. Charleux, J.-C. Sangleboeuf, P. Pilvin, T. Rouxel, G. Le Quilliec, Constitutive modeling of the densification process in silica glass under hydrostatic compression, Acta Mater. 62 (2014) 250–257.

[12] R. Lacroix, G. Kermouche, J. Teisseire, E. Barthel, Plastic deformation and residual stresses in amorphous silica pillars under uniaxial loading, Acta Mater. 60 (2012) 5555–5566.

[13] G. Kermouche, G. Guillonneau, J. Michler, J. Teisseire, E. Barthel, Perfectly plastic flow in silica glass, Acta Mater. 114 (2016) 146–153.

[14] F. M. Ernsberger, Role of Densification in Deformation of Glasses Under Point Loading, J. Am. Ceram. Soc. 51 (1968) 545–547.

[15] K. Peter, Densification and flow phenomena of glass in indentation experiments, J. Non. Cryst. Solids 5 (1970) 103–115.

[16] J. C. Lambropoulos, S. Xu, T. Fang, Constitutive Law for the Densification of Fused Silica, with Applications in Polishing and Microgrinding, J. Am. Ceram. Soc. 79 (1996) 1441–1452.

[17] K. Xin, J. C. Lambropoulos, Densification of Fused Silica : Effects on Nanoindentation, in: A. J. Marker III, E. G. Arthurs (Eds.), Inorg. Opt. Mater. II, volume 4102, SPIE, San Diego, CA, USA, 2000, pp. 112–121. doi:10.1117/12.405275.

[18] G. Kermouche, E. Barthel, D. Vandembroucq, P. Dubujet, Mechanical modelling of indentation-induced densification in amorphous silica, Acta Mater. 56 (2008) 3222–3228.

[19] K. Gadelrab, F. Bonilla, M. Chiesa, Densification modeling of fused silica under nanoindentation, J. Non. Cryst. Solids 358 (2012) 392–398.

[20] V. Keryvin, S. Gicquel, L. Charleux, J. P. Guin, M. Nivard, J. C. Sangleboeuf, Densification as the Only Mechanism at Stake during Indentation of Silica Glass?, Key Eng. Mater. 606 (2014) 53–60.

[21] A. Perriot, D. Vandembroucq, E. Barthel, V. Martinez, L. Grosvalet, C. Martinet, B. Champagnon, Raman Microspectroscopic Characterization of Amorphous Silica Plastic Behavior, J. Am. Ceram. Soc. 89 (2006) 596–601.

[22] Y.-F. Niu, K. Han, J.-P. Guin, Locally enhanced dissolution rate as a probe for nanocontact-induced densification in oxide glasses., Langmuir 28 (2012) 10733–40.

[23] W. Oliver, G. Pharr, An improved technique for determining hardness and elastic modulus using load and displacement sensing indentation experiments, J. Mater. Res. 7 (1992) 1564–1583.

[24] L. Charleux, V. Keryvin, L. Bizet, abapy: Abapy_v1.0, 2015. doi:10.5281/zenodo.17784.

[25] D. Tabor, The physical meaning of indentation and scratch hardness, Br. J. Appl. Phys. 7 (1956) 159.

[26] Y. T. Cheng, C. M. Cheng, Scaling, dimensional analysis, and indentation measurements, Mater. Sci. Eng. R Reports 44 (2004) 91–150.

[27] C.-S. Zha, R. Hemley, H.-K. Mao, T. Duffy, C. Meade, Acoustic velocities and refractive index of SiO2 glass to 57.5 GPa by Brillouin scattering, Phys. Rev. B 50 (1994) 13105–13112.

[28] T. Deschamps, J. Margueritat, C. Martinet, A. Mermet, B. Champagnon, Elastic moduli of permanently densified silica glasses., Sci. Rep. 4 (2014) 7193.

[29] R. F. Cook, G. M. Pharr, Direct Observation and Analysis of Indentation Cracking in Glasses and Ceramics, J. Am. Ceram. Soc. 73 (1990) 787–817.

[30] V. Keryvin, R. Crosnier, R. Laniel, V. H. Hoang, J.-C. Sanglebœuf, Indentation and scratching mechanisms of a ZrCuAlNi bulk metallic glass, J. Phys. D. Appl. Phys. 41 (2008) 074029.

[31] V. Keryvin, V. H. Hoang, J. Shen, Hardness, toughness, brittleness and cracking systems of an iron-based bulk metallic glass by indentation, Intermetallics 17 (2009) 211–217.

[32] G. Molnár, P. Ganster, A. Tanguy, E. Barthel, G. Kermouche, Densification dependent yield criteria for sodium silicate glasses - An atomistic simulation approach, Acta Mater. 111 (2016) 129–137.

[33] F. Yuan, L. Huang, Brittle to ductile transition in densified silica glass., Sci. Rep. 4 (2014) 5035.

[34] P. Donovan, Compressive deformation of amorphous Pd40Ni40P20, Mater. Sci. Eng. 98 (1988) 487–490.

[35] M. N. M. Patnaik, R. Narasimhan, U. Ramamurty, Spherical indentation response of metallic glasses, Acta Mater. 52 (2004) 3335–3345.

[36] V. Keryvin, Indentation as a probe for pressure sensitivity of metallic glasses., J. Phys.

Condens. Matter 20 (2008) 114119.

[37] K. E. Prasad, V. Keryvin, U. Ramamurty, Pressure sensitive flow and constraint factor in amorphous materials below glass transition, J. Mater. Res. 24 (2009) 890–897.

[38] B. Mantisi, G. Kermouche, E. Barthel, A. Tanguy, Impact of pressure on plastic yield in amorphous solids with open structure, Phys. Rev. E 93 (2016) 033001.

[39] X. Hernot, C. Moussa, O. Bartier, Study of the concept of representative strain and constraint factor introduced by Vickers indentation, Mech. Mater. 68 (2014) 1–14.

[40] V. Keryvin, Indentation of bulk metallic glasses: Relationships between shear bands observed around the prints and hardness, Acta Mater. 55 (2007) 2565–2578.

[41] V. Keryvin, K. Eswar Prasad, Y. Gueguen, J.-C. Sanglebœuf, U. Ramamurty, Temperature dependence of mechanical properties and pressure sensitivity in metallic glasses below glass transition, Philos. Mag. 88 (2008) 1773–1790.

[42] W. Oliver, G. Pharr, Measurement of hardness and elastic modulus by instrumented indentation: Advances in understanding and refinements to methodology, J. Mater. Res. 19 (2004) 3–20.

	C [GPa]	W_r/W_t [%]	δ_f [nm]	M [GPa]	H [GPa]	H_{IT} [GPa]
Pristine	106 ± 1	31.7 ± 0.1	486 ± 1	69 ± 1	8.40 ± 0.30	8.55 ± 0.05
Fully densified	153 ± 1	37.3 ± 1.2	412 ± 3	112 ± 2	11.5 ± 0.5	11.5 ± 1.0

Table 1. *Mechanical properties of pristine silica and fully densified silica from instrumented indentation testing. C is the loading pre-factor. W_r is the reversible work during unloading and W_t the total work involved in the test. δ_f is the residual penetration depth, and M is the indentation modulus of the material. H is Meyer's hardness measured from the residual imprint. H_{IT} is the IIT hardness following Oliver and Pharr's method [42].*

	E [GPa]	ν [-]	σ_y [GPa]	ϵ_y [%]	H/σ_y [-]
Pristine (from [12, 13])	72	0.15	$\sim$ 6.5-7.0	$\sim$ 9.5	1.2-1.3
Fully densified (this work)	106 ± 1	0.22	6.5	6.1	1.89 ± 0.08

Table 2. *Mechanical properties of both pristine and fully densified silica glass. E, ν, σ_y and ϵ_y are respectively Young's modulus, Poisson's ratio, compressive yield strength and compressive yield strain in pure compression. The ratio hardness to compressive yield strength is also reported.*

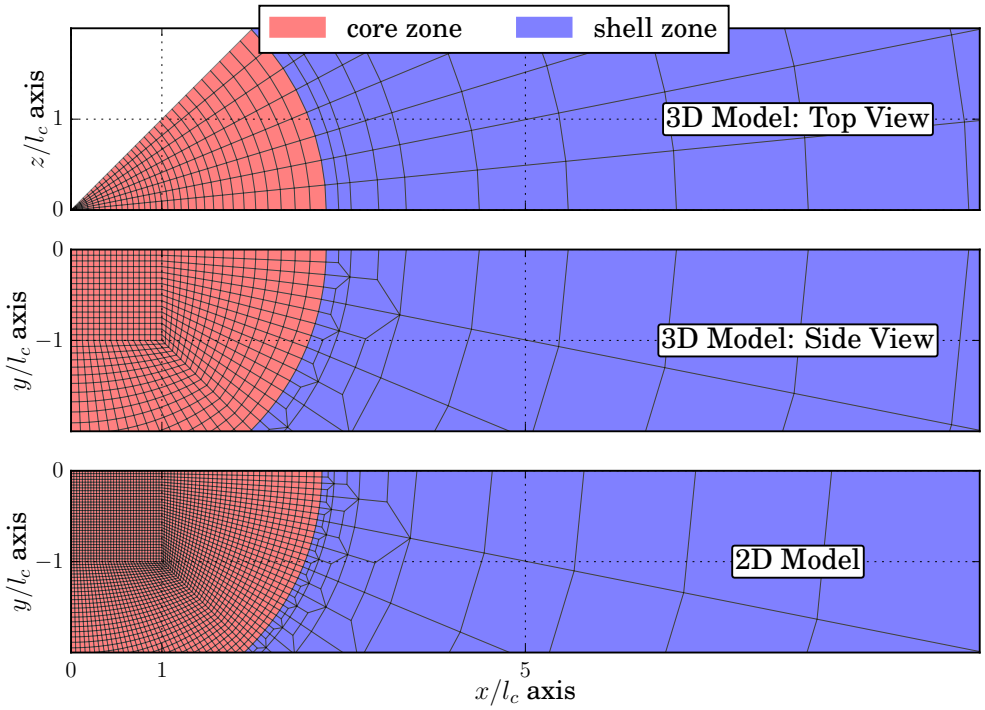

Figure 1. *View of the 2D and 3D meshes used in the FEM simulations for the material close to the contact location. The core and shell zones are represented respectively in red and blue. The 3D mesh is a 45° swept version of a coarse 2D mesh. l_c stands for the horizontal length of the core zone.*

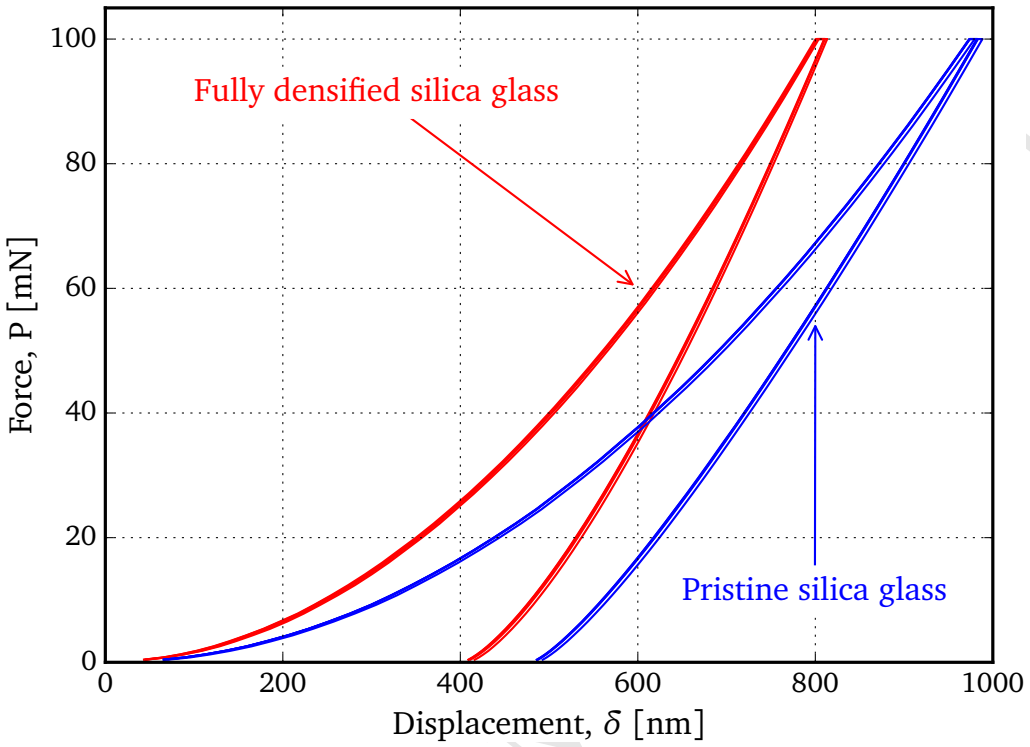

Figure 2. *Nano-indentation force-displacements curves for pristine silica glass and fully densified silica glass. Five tests are carried out for each type, and experimental reproducibility is confirmed.*

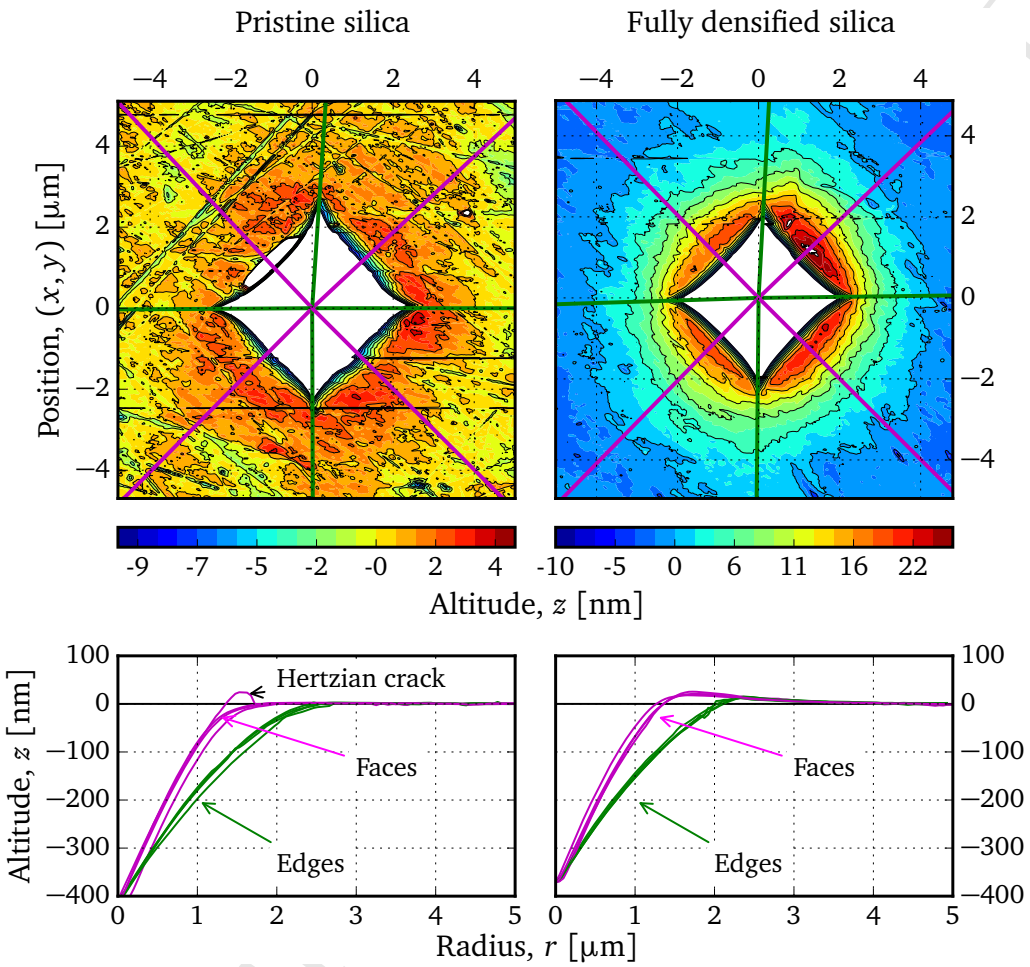

Figure 3. *Topography AFM images (5×5 μm², top) presenting the residual imprints of a Vickers indentation (100 mN) for the pristine silica glass (left) and the fully densified silica (right). For sake of presentation the altitudes below -10 nm are masked (white part). For pristine silica (used only for comparison), edge cracks are visible. For fully densified silica, colors different from blue are indicative of a residual pile-up ($z > 0$). A unusual long range residual pile-up all around the imprint is observed. Altitude profiles are then extracted (bottom) along the four edges (green) and the four faces (magenta) for both specimens. No piling-up is visible along the faces and the edges for pristine silica. Piling-up is present along the faces and the edges for fully densified silica silica.*

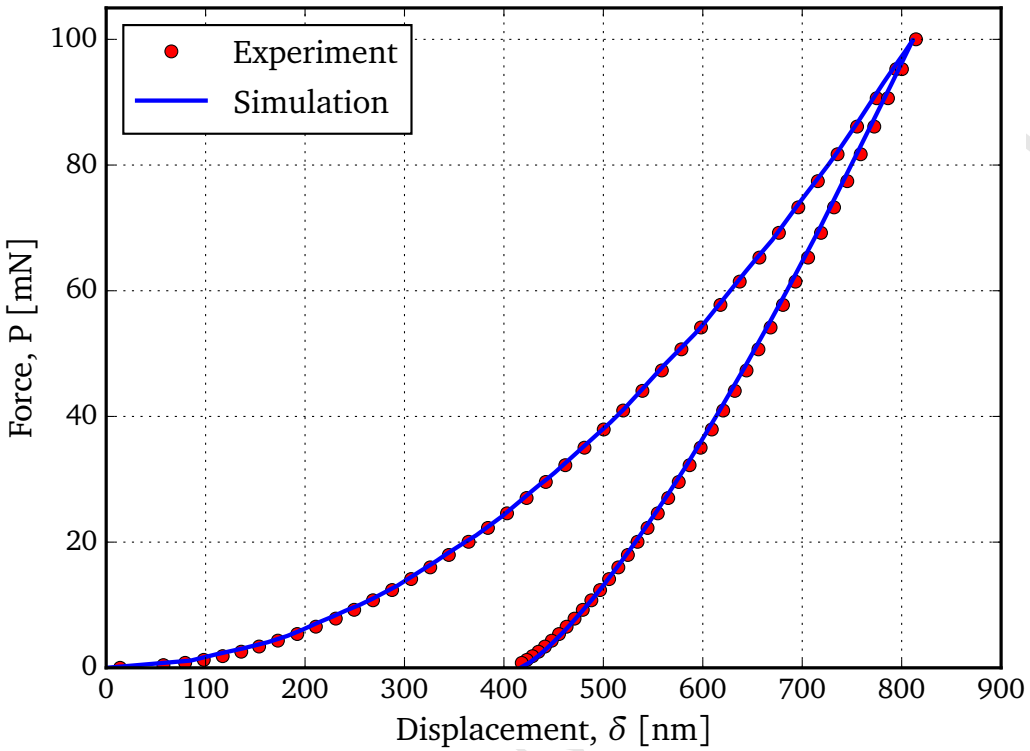

Figure 4. *Force-displacement curves of the nano-indentation test in fully densified silica at 100 mN. Comparison between experimental results and numerical simulation (3D FEA).*

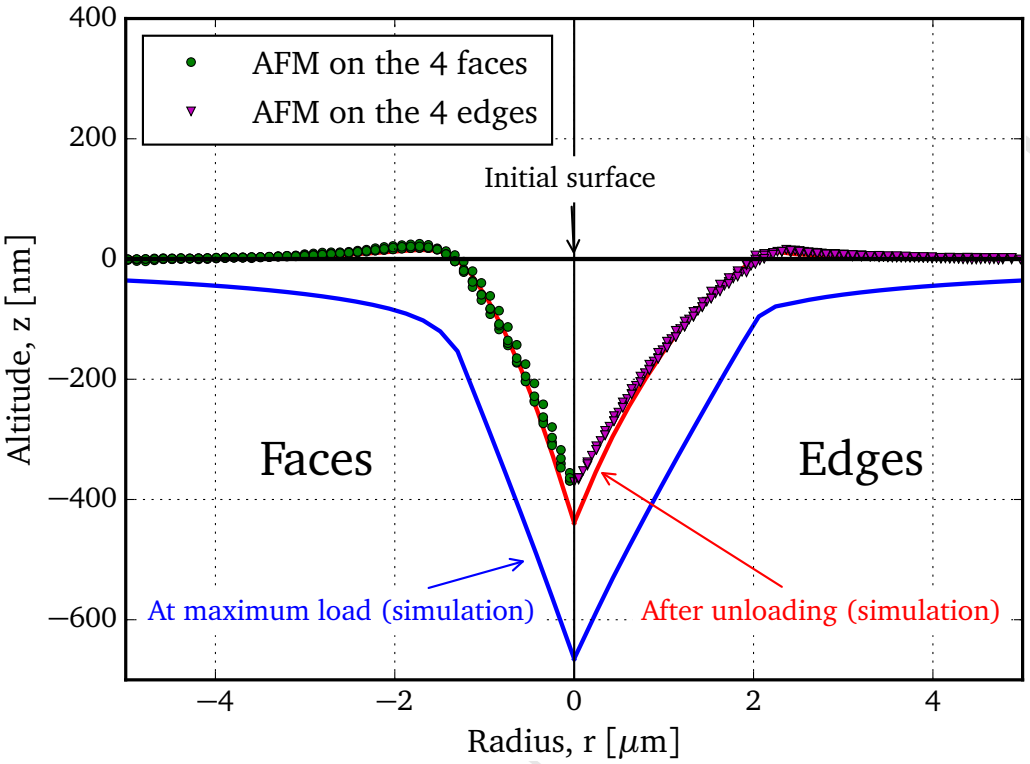

Figure 5. *Comparison between experimental (AFM) results and numerical simulations (3D FEA) of the residual imprint profile in fully densified silica indented at 100 mN by a Vickers pyramid. The four experimental profiles are plotted together for sake of presentation either along the edges (right) or the faces (left). The profiles at maximum load, as predicted by the simulations (blue color), indicate that there is no piling-up during loading.*

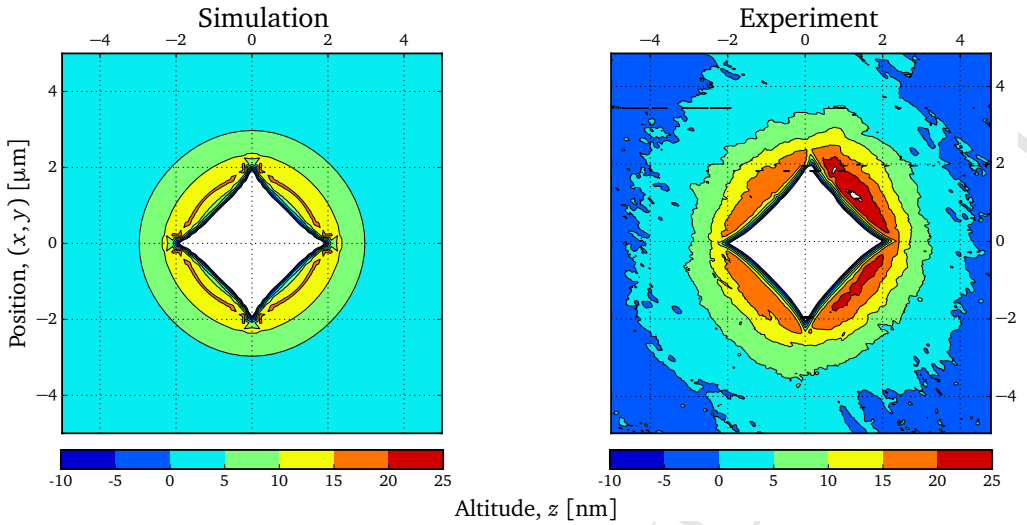

Figure 6. *Comparison between experimental (AFM, right) results and numerical simulations (3D FEA, left) of the residual imprint profile in fully densified silica indented at 100 mN by a Vickers pyramid. Topography view.*

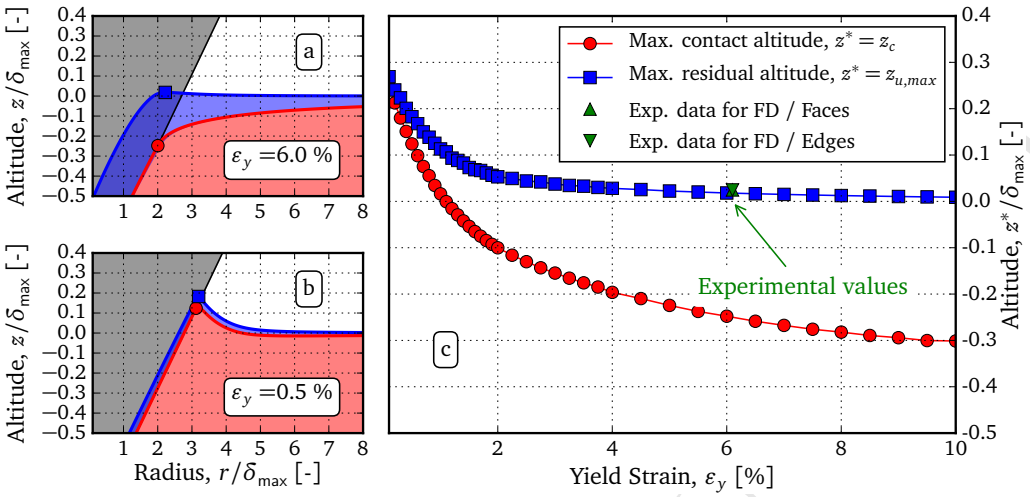

Figure 7. *Axisymmetric numerical simulation results with a von Mises constitutive model. On the left side, two states of the simulation are superimposed: at maximum load (maximum penetration depth δ_{max}) and after complete unloading. The indenter is filled in grey (under load) while the sample is filled in red (under load) or blue (after unloading). The red circle marker represents the highest point in contact under load z_c, while the blue square marker represents the highest point of the residual imprint $z_{u,max}$. **(a)** corresponds to a yield strain $\varepsilon_y = 0.5\%$, while **(b)** is for $\varepsilon_y = 6\%$. The values of z_c and $z_{u,max}$, with respect to δ_{max}, are represented as a function of ε_y on the right side **(c)**. Piling-up (positive values of the relative depth) and sinking-in (negative values) during loading and unloading are visible. Experimental values (3D) for fully densified silica (FD) are superimposed for the faces and the edges.*

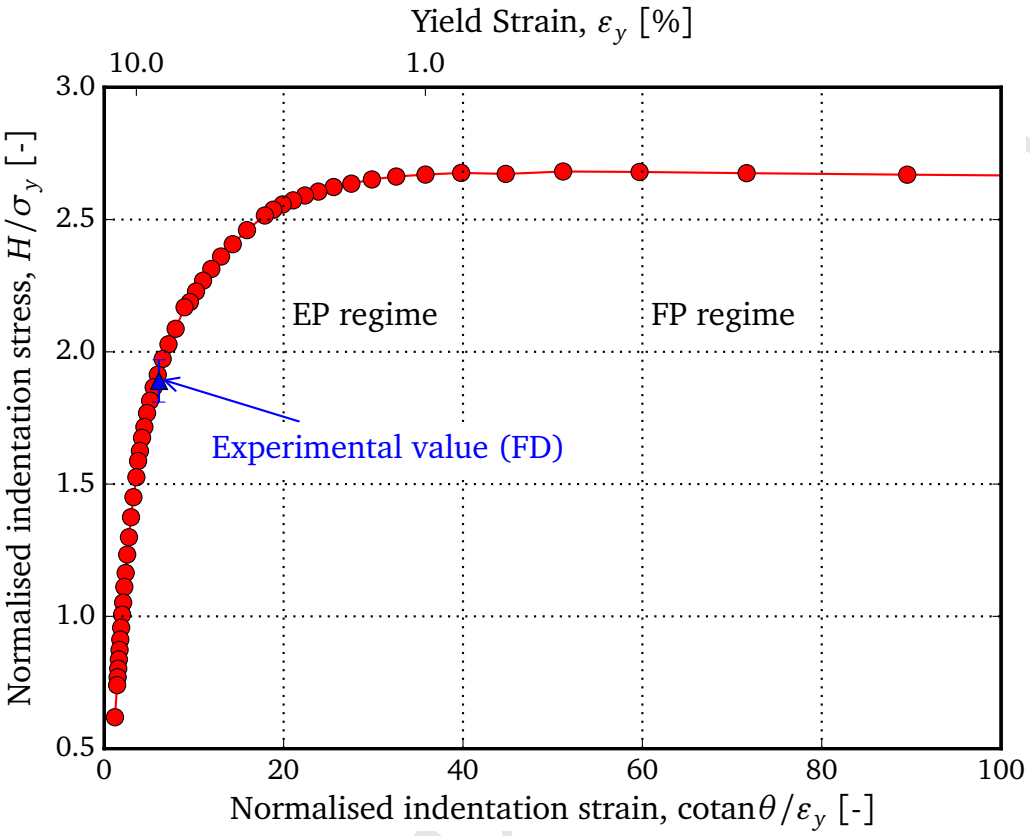

Figure 8. *Normalised indentation stress (H is Meyer's hardness and σ_y is the material's yield strength) versus normalised indentation strain (cotanθ, where θ is the half angle of the equivalent cone, here 70.27°; ϵ_y is the material's yield strain). Numerical simulations (2D, $\nu = 0.22$) allow to distinguish between the fully plastic regime (FP), for which H/σ_y is a constant $c = 2.65$ and the elasto-plastic regime (EP), for which H/σ_y is an increasing function of $1/\epsilon_y$. The experimental value for fully densified silica (FD) is superimposed.*